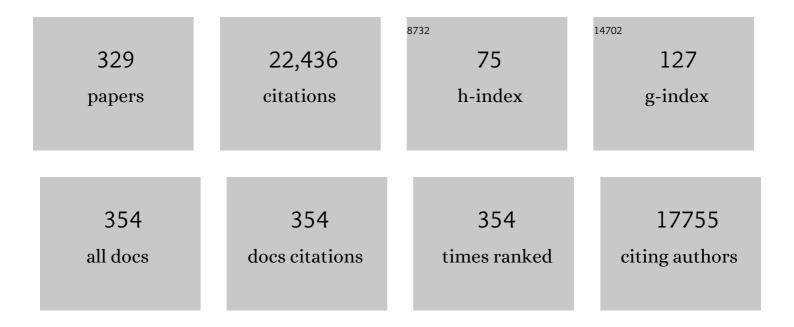
Lawrence L Wald

List of Publications by Year in descending order

Source: https://exaly.com/author-pdf/1570777/publications.pdf Version: 2024-02-01



LAWDENCE | WALD

#	Article	IF	CITATIONS
1	Blippedâ€controlled aliasing in parallel imaging for simultaneous multislice echo planar imaging with reduced <i>g</i> â€factor penalty. Magnetic Resonance in Medicine, 2012, 67, 1210-1224.	1.9	1,144
2	A computational atlas of the hippocampal formation using ex vivo, ultra-high resolution MRI: Application to adaptive segmentation of in vivo MRI. NeuroImage, 2015, 115, 117-137.	2.1	939
3	Comparison of physiological noise at 1.5 T, 3 T and 7 T and optimization of fMRI acquisition parameters. NeuroImage, 2005, 26, 243-250.	2.1	598
4	Pushing the limits of in vivo diffusion MRI for the Human Connectome Project. Neurolmage, 2013, 80, 220-233.	2.1	460
5	Automated segmentation of hippocampal subfields from ultraâ€high resolution in vivo MRI. Hippocampus, 2009, 19, 549-557.	0.9	381
6	Laminar analysis of 7T BOLD using an imposed spatial activation pattern in human V1. NeuroImage, 2010, 52, 1334-1346.	2.1	378
7	32-channel 3 Tesla receive-only phased-array head coil with soccer-ball element geometry. Magnetic Resonance in Medicine, 2006, 56, 216-223.	1.9	347
8	Visual word processing and experiential origins of functional selectivity in human extrastriate cortex. Proceedings of the National Academy of Sciences of the United States of America, 2007, 104, 9087-9092.	3.3	325
9	Brain Genomics Superstruct Project initial data release with structural, functional, and behavioral measures. Scientific Data, 2015, 2, 150031.	2.4	318
10	Hyperpolarized 13C MRI: Path to Clinical Translation in Oncology. Neoplasia, 2019, 21, 1-16.	2.3	316
11	Stereopsis Activates V3A and Caudal Intraparietal Areas in Macaques and Humans. Neuron, 2003, 39, 555-568.	3.8	309
12	The Human Connectome Project and beyond: Initial applications of 300mT/m gradients. NeuroImage, 2013, 80, 234-245.	2.1	309
13	Improving diffusion MRI using simultaneous multi-slice echo planar imaging. NeuroImage, 2012, 63, 569-580.	2.1	303
14	Three dimensional echo-planar imaging at 7 Tesla. NeuroImage, 2010, 51, 261-266.	2.1	266
15	Repeated fMRI Using Iron Oxide Contrast Agent in Awake, Behaving Macaques at 3 Tesla. NeuroImage, 2002, 16, 283-294.	2.1	250
16	Theory and application of array coils in MR spectroscopy. , 1997, 10, 394-410.		247
17	96â€Channel receiveâ€only head coil for 3 Tesla: Design optimization and evaluation. Magnetic Resonance in Medicine, 2009, 62, 754-762.	1.9	237
18	Parallel imaging reconstruction using automatic regularization. Magnetic Resonance in Medicine, 2004, 51, 559-567.	1.9	232

#	Article	IF	CITATIONS
19	Interslice leakage artifact reduction technique for simultaneous multislice acquisitions. Magnetic Resonance in Medicine, 2014, 72, 93-102.	1.9	229
20	Organization of high-level visual cortex in human infants. Nature Communications, 2017, 8, 13995.	5.8	224
21	Accurate prediction of V1 location from cortical folds in a surface coordinate system. NeuroImage, 2008, 39, 1585-1599.	2.1	221
22	3T phased array MRI improves the presurgical evaluation in focal epilepsies: A prospective study. Neurology, 2005, 65, 1026-1031.	1.5	217
23	MGH–USC Human Connectome Project datasets with ultra-high b-value diffusion MRI. NeuroImage, 2016, 124, 1108-1114.	2.1	209
24	A 64â€channel 3T array coil for accelerated brain MRI. Magnetic Resonance in Medicine, 2013, 70, 248-258.	1.9	202
25	Optogenetically Induced Behavioral and Functional Network Changes in Primates. Current Biology, 2012, 22, 1722-1726.	1.8	196
26	Magnitude least squares optimization for parallel radio frequency excitation design demonstrated at 7 Tesla with eight channels. Magnetic Resonance in Medicine, 2008, 59, 908-915.	1.9	181
27	Waveâ€CAIPI for highly accelerated 3D imaging. Magnetic Resonance in Medicine, 2015, 73, 2152-2162.	1.9	180
28	7 Tesla MRI of the ex vivo human brain at 100 micron resolution. Scientific Data, 2019, 6, 244.	2.4	179
29	Effects of image reconstruction on fiber orientation mapping from multichannel diffusion MRI: Reducing the noise floor using SENSE. Magnetic Resonance in Medicine, 2013, 70, 1682-1689.	1.9	169
30	Physiological noise and signal-to-noise ratio in fMRI with multi-channel array coils. NeuroImage, 2011, 55, 597-606.	2.1	167
31	Visual Field Map Clusters in Macaque Extrastriate Visual Cortex. Journal of Neuroscience, 2009, 29, 7031-7039.	1.7	158
32	Serial proton magnetic resonance spectroscopy imaging of glioblastoma multiforme after brachytherapy. Journal of Neurosurgery, 1997, 87, 525-534.	0.9	155
33	Parallel RF transmission with eight channels at 3 Tesla. Magnetic Resonance in Medicine, 2006, 56, 1163-1171.	1.9	148
34	Massively parallel MRI detector arrays. Journal of Magnetic Resonance, 2013, 229, 75-89.	1.2	143
35	A 128-channel receive-only cardiac coil for highly accelerated cardiac MRI at 3 Tesla. Magnetic Resonance in Medicine, 2008, 59, 1431-1439.	1.9	142
36	Sliceâ€selective RF pulses for in vivo <i>B</i> inhomogeneity mitigation at 7 tesla using parallel RF excitation with a 16â€element coil. Magnetic Resonance in Medicine, 2008, 60, 1422-1432.	1.9	140

#	Article	IF	CITATIONS
37	Multislice perfusion and perfusion territory imaging in humans with separate label and image coils. Magnetic Resonance in Medicine, 1999, 41, 1093-1098.	1.9	135
38	Surface based analysis of diffusion orientation for identifying architectonic domains in the in vivo human cortex. NeuroImage, 2013, 69, 87-100.	2.1	134
39	Highâ€resolution in vivo diffusion imaging of the human brain with generalized slice dithered enhanced resolution: Simultaneous multislice (g <scp>S</scp> liderâ€ <scp>SMS</scp>). Magnetic Resonance in Medicine, 2018, 79, 141-151.	1.9	134
40	T2* mapping and B0 orientation-dependence at 7T reveal cyto- and myeloarchitecture organization of the human cortex. Neurolmage, 2012, 60, 1006-1014.	2.1	133
41	Low ost and portable MRI. Journal of Magnetic Resonance Imaging, 2020, 52, 686-696.	1.9	128
42	Phased array detectors and an automated intensity-correction algorithm for high-resolution MR imaging of the human brain. Magnetic Resonance in Medicine, 1995, 34, 433-439.	1.9	126
43	Effect of spatial smoothing on physiological noise in high-resolution fMRI. Neurolmage, 2006, 32, 551-557.	2.1	125
44	Identification of discrete functional subregions of the human periaqueductal gray. Proceedings of the United States of America, 2013, 110, 17101-17106.	3.3	125
45	Fast image reconstruction with L2â€regularization. Journal of Magnetic Resonance Imaging, 2014, 40, 181-191.	1.9	125
46	Twoâ€dimensional imaging in a lightweight portable MRI scanner without gradient coils. Magnetic Resonance in Medicine, 2015, 73, 872-883.	1.9	125
47	Sizeâ€optimized 32â€channel brain arrays for 3 T pediatric imaging. Magnetic Resonance in Medicine, 2011, 66, 1777-1787.	1.9	118
48	Signal-to-noise ratio and spectral linewidth improvements between 1.5 and 7 Tesla in proton echo-planar spectroscopic imaging. Magnetic Resonance in Medicine, 2006, 56, 1200-1210.	1.9	115
49	Variability and anatomical specificity of the orbitofrontothalamic fibers of passage in the ventral capsule/ventral striatum (VC/VS): precision care for patient-specific tractography-guided targeting of deep brain stimulation (DBS) in obsessive compulsive disorder (OCD). Brain Imaging and Behavior, 2016, 10, 1054-1067.	1.1	115
50	In vivo detection of GABA in human brain using a localized double-quantum filter technique. Magnetic Resonance in Medicine, 1997, 37, 366-371.	1.9	113
51	Reducing sensitivity losses due to respiration and motion in accelerated echo planar imaging by reordering the autocalibration data acquisition. Magnetic Resonance in Medicine, 2016, 75, 665-679.	1.9	113
52	Improved magnetic resonance fingerprinting reconstruction with lowâ€rank and subspace modeling. Magnetic Resonance in Medicine, 2018, 79, 933-942.	1.9	113
53	Detection of entorhinal layer II using Tesla magnetic resonance imaging. Annals of Neurology, 2005, 57, 489-494.	2.8	110
54	Fast quantitative susceptibility mapping with L1â€regularization and automatic parameter selection. Magnetic Resonance in Medicine, 2014, 72, 1444-1459.	1.9	110

#	Article	IF	CITATIONS
55	A 32â€channel combined RF and <i>B₀</i> shim array for 3T brain imaging. Magnetic Resonance in Medicine, 2016, 75, 441-451.	1.9	106
56	Frontal connections and cognitive changes in normal aging rhesus monkeys: A DTI study. Neurobiology of Aging, 2007, 28, 1556-1567.	1.5	105
57	In vivo B 0 field shimming methods for MRI at 7 T. NeuroImage, 2018, 168, 71-87.	2.1	105
58	Modulation of brain and serum glutamatergic concentrations following a switch from conventional neuroleptics to olanzapine. Biological Psychiatry, 2002, 51, 493-497.	0.7	104
59	A portable scanner for magnetic resonance imaging of the brain. Nature Biomedical Engineering, 2021, 5, 229-239.	11.6	103
60	Maximum Likelihood Reconstruction for Magnetic Resonance Fingerprinting. IEEE Transactions on Medical Imaging, 2016, 35, 1812-1823.	5.4	99
61	In vivo tracing of major rat brain pathways using manganese-enhanced magnetic resonance imaging and three-dimensional digital atlasing. NeuroImage, 2003, 20, 1591-1600.	2.1	98
62	Three-dimensional magnetic resonance spectroscopic imaging of histologically confirmed brain tumors. Magnetic Resonance Imaging, 2001, 19, 89-101.	1.0	95
63	The impact of gradient strength on in vivo diffusion MRI estimates of axon diameter. NeuroImage, 2015, 106, 464-472.	2.1	95
64	Predicting the location of entorhinal cortex from MRI. NeuroImage, 2009, 47, 8-17.	2.1	94
65	Dynamic magnetic resonance inverse imaging of human brain function. Magnetic Resonance in Medicine, 2006, 56, 787-802.	1.9	93
66	Dissociation of neural regions associated with anticipatory versus consummatory phases of incentive processing. Psychophysiology, 2008, 45, 36-49.	1.2	92
67	RF-induced heating in tissue near bilateral DBS implants during MRI at 1.5†T and 3T: The role of surgical lead management. NeuroImage, 2019, 184, 566-576.	2.1	92
68	Optimal Experiment Design for Magnetic Resonance Fingerprinting: Cramér-Rao Bound Meets Spin Dynamics. IEEE Transactions on Medical Imaging, 2019, 38, 844-861.	5.4	89
69	Eight-channel phased array coil and detunable TEM volume coil for 7 T brain imaging. Magnetic Resonance in Medicine, 2005, 54, 235-240.	1.9	88
70	Real diffusion-weighted MRI enabling true signal averaging and increased diffusion contrast. NeuroImage, 2015, 122, 373-384.	2.1	88
71	Fast group matching for MR fingerprinting reconstruction. Magnetic Resonance in Medicine, 2015, 74, 523-528.	1.9	87
72	3D MR fingerprinting with accelerated stack-of-spirals and hybrid sliding-window and GRAPPA reconstruction. Neurolmage, 2017, 162, 13-22.	2.1	87

#	Article	IF	CITATIONS
73	Quantitative comparison of cortical surface reconstructions from MP2RAGE and multi-echo MPRAGE data at 3 and 7T. NeuroImage, 2014, 90, 60-73.	2.1	85
74	Design of Sparse Halbach Magnet Arrays for Portable MRI Using a Genetic Algorithm. IEEE Transactions on Magnetics, 2018, 54, 1-12.	1.2	85
75	Proton spectroscopic imaging of the human brain using phased array detectors. Magnetic Resonance in Medicine, 1995, 34, 440-445.	1.9	84
76	Local specific absorption rate (SAR), global SAR, transmitter power, and excitation accuracy tradeâ€offs in low flipâ€angle parallel transmit pulse design. Magnetic Resonance in Medicine, 2014, 71, 1446-1457.	1.9	84
77	High spatial resolution1H-MRSI and segmented MRI of cortical gray matter and subcortical white matter in three regions of the human brain. Magnetic Resonance in Medicine, 1999, 41, 21-29.	1.9	82
78	Predicting the location of human perirhinal cortex, Brodmann's area 35, from MRI. NeuroImage, 2013, 64, 32-42.	2.1	81
79	Local <scp>SAR</scp> near deep brain stimulation (<scp>DBS</scp>) electrodes at 64 and 127 <scp>MH</scp> z: A simulation study of the effect of extracranial loops. Magnetic Resonance in Medicine, 2017, 78, 1558-1565.	1.9	81
80	Volume MRI and MRSI techniques for the quantitation of treatment response in brain tumors: Presentation of a detailed case study. Journal of Magnetic Resonance Imaging, 1997, 7, 1146-1152.	1.9	80
81	Direct parallel image reconstructions for spiral trajectories using CRAPPA. Magnetic Resonance in Medicine, 2006, 56, 317-326.	1.9	80
82	Sensitivity-encoded (SENSE) proton echo-planar spectroscopic imaging (PEPSI) in the human brain. Magnetic Resonance in Medicine, 2007, 57, 249-257.	1.9	78
83	Echo planar timeâ€resolved imaging (EPTI). Magnetic Resonance in Medicine, 2019, 81, 3599-3615.	1.9	75
84	The Challenge of Connecting the Dots in the B.R.A.I.N Neuron, 2013, 80, 270-274.	3.8	73
85	Local SAR in parallel transmission pulse design. Magnetic Resonance in Medicine, 2012, 67, 1566-1578.	1.9	71
86	Accelerated volumetric MRI with a SENSE/GRAPPA combination. Journal of Magnetic Resonance Imaging, 2006, 24, 444-450.	1.9	70
87	Feasibility of using linearly polarized rotating birdcage transmitters and close-fitting receive arrays in MRI to reduce SAR in the vicinity of deep brain simulation implants. Magnetic Resonance in Medicine, 2017, 77, 1701-1712.	1.9	70
88	In vivo mapping of human spinal cord microstructure at 300 mT/m. NeuroImage, 2015, 118, 494-507.	2.1	69
89	A wavelet-based approximation of surface coil sensitivity profiles for correction of image intensity inhomogeneity and parallel imaging reconstruction. Human Brain Mapping, 2003, 19, 96-111.	1.9	68
90	Fast sliceâ€selective radioâ€frequency excitation pulses for mitigating <i>B</i> inhomogeneity in the human brain at 7 Tesla. Magnetic Resonance in Medicine, 2008, 59, 1355-1364.	1.9	68

#	Article	IF	CITATIONS
91	RARE/turbo spin echo imaging with simultaneous multislice Wave-CAIPI. Magnetic Resonance in Medicine, 2015, 73, 929-938.	1.9	68
92	Toward an <i>In Vivo</i> Neuroimaging Template of Human Brainstem Nuclei of the Ascending Arousal, Autonomic, and Motor Systems. Brain Connectivity, 2015, 5, 597-607.	0.8	68
93	Specific absorption rate studies of the parallel transmission of innerâ€volume excitations at 7T. Journal of Magnetic Resonance Imaging, 2008, 28, 1005-1018.	1.9	67
94	Sparsity-Promoting Calibration for GRAPPA Accelerated Parallel MRI Reconstruction. IEEE Transactions on Medical Imaging, 2013, 32, 1325-1335.	5.4	67
95	Network Accelerated Motion Estimation and Reduction (NAMER): Convolutional neural network guided retrospective motion correction using a separable motion model. Magnetic Resonance in Medicine, 2019, 82, 1452-1461.	1.9	67
96	Accelerated diffusion spectrum imaging with compressed sensing using adaptive dictionaries. Magnetic Resonance in Medicine, 2012, 68, 1747-1754.	1.9	66
97	Toward 20ÂT magnetic resonance for human brain studies: opportunities for discovery and neuroscience rationale. Magnetic Resonance Materials in Physics, Biology, and Medicine, 2016, 29, 617-639.	1.1	66
98	g-Ratio weighted imaging of the human spinal cord in vivo. NeuroImage, 2017, 145, 11-23.	2.1	66
99	Hippocampal Volume, PTSD, and Alcoholism in Combat Veterans. American Journal of Psychiatry, 2006, 163, 674-681.	4.0	65
100	Lactate detection at 3T: Compensating J coupling effects with BASING. Journal of Magnetic Resonance Imaging, 1999, 9, 732-737.	1.9	63
101	Targeted imaging of human endothelial-specific marker in a model of adoptive cell transfer. Laboratory Investigation, 2006, 86, 599-609.	1.7	63
102	Accelerated proton echo planar spectroscopic imaging (PEPSI) using GRAPPA with a 32â€channel phasedâ€array coil. Magnetic Resonance in Medicine, 2008, 59, 989-998.	1.9	63
103	Comparison of Cardiac MRI on 1.5 and 3.0 Tesla Clinical Whole Body Systems. Investigative Radiology, 2003, 38, 436-442.	3.5	62
104	Improving parallel imaging by jointly reconstructing multi ontrast data. Magnetic Resonance in Medicine, 2018, 80, 619-632.	1.9	62
105	The ultimate signalâ€ŧoâ€noise ratio in realistic body models. Magnetic Resonance in Medicine, 2017, 78, 1969-1980.	1.9	61
106	In vivo functional connectome of human brainstem nuclei of the ascending arousal, autonomic, and motor systems by high spatial resolution 7-Tesla fMRI. Magnetic Resonance Materials in Physics, Biology, and Medicine, 2016, 29, 451-462.	1.1	59
107	Construction and modeling of a reconfigurable MRI coil for lowering SAR in patients with deep brain stimulation implants. NeuroImage, 2017, 147, 577-588.	2.1	58
108	Connectome 2.0: Developing the next-generation ultra-high gradient strength human MRI scanner for bridging studies of the micro-, meso- and macro-connectome. NeuroImage, 2021, 243, 118530.	2.1	58

#	Article	IF	CITATIONS
109	Comparison of simulated parallel transmit body arrays at 3 T using excitation uniformity, global SAR, local SAR, and power efficiency metrics. Magnetic Resonance in Medicine, 2015, 73, 1137-1150.	1.9	57
110	Automatic cortical surface reconstruction of high-resolution T1 echo planar imaging data. NeuroImage, 2016, 134, 338-354.	2.1	57
111	Targeting of White Matter Tracts with Transcranial Magnetic Stimulation. Brain Stimulation, 2014, 7, 80-84.	0.7	56
112	Parallel transmit pulse design for patients with deep brain stimulation implants. Magnetic Resonance in Medicine, 2015, 73, 1896-1903.	1.9	56
113	Age-related alterations in axonal microstructure in the corpus callosum measured by high-gradient diffusion MRI. NeuroImage, 2019, 191, 325-336.	2.1	55
114	High-gradient diffusion MRI reveals distinct estimates of axon diameter index within different white matter tracts in the in vivo human brain. Brain Structure and Function, 2020, 225, 1277-1291.	1.2	55
115	Sparsity-Enforced Slice-Selective MRI RF Excitation Pulse Design. IEEE Transactions on Medical Imaging, 2008, 27, 1213-1229.	5.4	54
116	Broadband slab selection with B mitigation at 7T via parallel spectralâ€spatial excitation. Magnetic Resonance in Medicine, 2009, 61, 493-500.	1.9	54
117	Accelerating magnetic resonance fingerprinting (MRF) using t-blipped simultaneous multislice (SMS) acquisition. Magnetic Resonance in Medicine, 2016, 75, 2078-2085.	1.9	54
118	Degenerate mode band-pass birdcage coil for accelerated parallel excitation. Magnetic Resonance in Medicine, 2007, 57, 1148-1158.	1.9	53
119	Performance evaluation of a 32â€element head array with respect to the ultimate intrinsic SNR. NMR in Biomedicine, 2010, 23, 142-151.	1.6	53
120	Investigating the Capability to Resolve Complex White Matter Structures with High <i>b</i> -Value Diffusion Magnetic Resonance Imaging on the MGH-USC Connectom Scanner. Brain Connectivity, 2014, 4, 718-726.	0.8	53
121	White matter compartment models for in vivo diffusion MRI at 300 mT/m. NeuroImage, 2015, 118, 468-483.	2.1	53
122	Wave AIPI for highly accelerated MPâ€RAGE imaging. Magnetic Resonance in Medicine, 2018, 79, 401-406.	1.9	53
123	Nineteen-channel receive array and four-channel transmit array coil for cervical spinal cord imaging at 7T. Magnetic Resonance in Medicine, 2014, 72, 291-300.	1.9	52
124	Rapid multi-orientation quantitative susceptibility mapping. NeuroImage, 2016, 125, 1131-1141.	2.1	52
125	The MR Cap: A singleâ€sided MRI system designed for potential pointâ€ofâ€eare limited fieldâ€ofâ€view brain imaging. Magnetic Resonance in Medicine, 2019, 82, 1946-1960.	1.9	52
126	Design considerations and coil comparisons for 7 T brain imaging. Applied Magnetic Resonance, 2005, 29, 19-37.	0.6	51

#	Article	IF	CITATIONS
127	Simultaneous multislice excitation by parallel transmission. Magnetic Resonance in Medicine, 2014, 71, 1416-1427.	1.9	51
128	Design of parallel transmission pulses for simultaneous multislice with explicit control for peak power and local specific absorption rate. Magnetic Resonance in Medicine, 2015, 73, 1946-1953.	1.9	51
129	Prediction of peripheral nerve stimulation thresholds of MRI gradient coils using coupled electromagnetic and neurodynamic simulations. Magnetic Resonance in Medicine, 2019, 81, 686-701.	1.9	51
130	Reconfigurable MRI technology for low-SAR imaging of deep brain stimulation at 3T: Application in bilateral leads, fully-implanted systems, and surgically modified lead trajectories. NeuroImage, 2019, 199, 18-29.	2.1	51
131	A technique for detecting GABA in the human brain with PRESS localization and optimized refocusing spectral editing radiofrequency pulses. Magnetic Resonance in Medicine, 1996, 36, 458-461.	1.9	50
132	Singleâ€step quantitative susceptibility mapping with variational penalties. NMR in Biomedicine, 2017, 30, e3570.	1.6	50
133	Axon diameter index estimation independent of fiber orientation distribution using high-gradient diffusion MRI. NeuroImage, 2020, 222, 117197.	2.1	49
134	Functional MRI using regularized parallel imaging acquisition. Magnetic Resonance in Medicine, 2005, 54, 343-353.	1.9	48
135	Hippocampal volume, PTSD, and alcoholism in combat veterans. American Journal of Psychiatry, 2006, 163, 674-81.	4.0	48
136	A low power radiofrequency pulse for simultaneous multislice excitation and refocusing. Magnetic Resonance in Medicine, 2014, 72, 949-958.	1.9	47
137	Autocalibrated waveâ€ <scp>CAIPI</scp> reconstruction; Joint optimization of kâ€space trajectory and parallel imaging reconstruction. Magnetic Resonance in Medicine, 2017, 78, 1093-1099.	1.9	47
138	An implanted 8-channel array coil for high-resolution macaque MRI at 3T. NeuroImage, 2012, 62, 1529-1536.	2.1	46
139	Reducing RF-Induced Heating Near Implanted Leads Through High-Dielectric Capacitive Bleeding of Current (CBLOC). IEEE Transactions on Microwave Theory and Techniques, 2019, 67, 1265-1273.	2.9	46
140	Chronic citicoline increases phosphodiesters in the brains of healthy older subjects: an in vivo phosphorus magnetic resonance spectroscopy study. Psychopharmacology, 2002, 161, 248-254.	1.5	45
141	Event-related single-shot volumetric functional magnetic resonance inverse imaging of visual processing. Neurolmage, 2008, 42, 230-247.	2.1	45
142	32â€Channel RF coil optimized for brain and cervical spinal cord at 3 T. Magnetic Resonance in Medicine, 2011, 66, 1198-1208.	1.9	45
143	Predicting Magnetostimulation Thresholds in the Peripheral Nervous System using Realistic Body Models. Scientific Reports, 2017, 7, 5316.	1.6	45
144	A probabilistic template of human mesopontine tegmental nuclei from in vivo 7 T MRI. NeuroImage, 2018, 170, 222-230.	2.1	45

#	Article	IF	CITATIONS
145	TArgeted Motion Estimation and Reduction (TAMER): Data Consistency Based Motion Mitigation for MRI Using a Reduced Model Joint Optimization. IEEE Transactions on Medical Imaging, 2018, 37, 1253-1265.	5.4	44
146	Highlyâ€accelerated volumetric brain examination using optimized waveâ€CAIPI encoding. Journal of Magnetic Resonance Imaging, 2019, 50, 961-974.	1.9	44
147	Reconfigurable MRI coil technology can substantially reduce RF heating of deep brain stimulation implants: First in-vitro study of RF heating reduction in bilateral DBS leads at 1.5 T. PLoS ONE, 2019, 14, e0220043.	1.1	43
148	Nonstationary noise estimation in functional MRI. NeuroImage, 2005, 28, 890-903.	2.1	42
149	Globally conditioned Granger causality in brain–brain and brain–heart interactions: a combined heart rate variability/ultra-high-field (7 T) functional magnetic resonance imaging study. Philosophical Transactions Series A, Mathematical, Physical, and Engineering Sciences, 2016, 374, 20150185.	1.6	42
150	Changes in the specific absorption rate (SAR) of radiofrequency energy in patients with retained cardiac leads during MRI at 1.5T and 3T. Magnetic Resonance in Medicine, 2019, 81, 653-669.	1.9	42
151	In vivo GABA+ measurement at 1.5T using a PRESS-localized double quantum filter. Magnetic Resonance in Medicine, 2002, 48, 233-241.	1.9	41
152	High-flip-angle slice-selective parallel RF transmission with 8 channels at 7T. Journal of Magnetic Resonance, 2008, 195, 76-84.	1.2	41
153	Stimulus-induced Rotary Saturation (SIRS): A potential method for the detection of neuronal currents with MRI. NeuroImage, 2008, 42, 1357-1365.	2.1	41
154	Slice accelerated diffusionâ€weighted imaging at ultraâ€high field strength. Magnetic Resonance in Medicine, 2014, 71, 1518-1525.	1.9	41
155	Intracortical smoothing of small-voxel fMRI data can provide increased detection power without spatial resolution losses compared to conventional large-voxel fMRI data. NeuroImage, 2019, 189, 601-614.	2.1	41
156	CENTS: Cortical enhanced neonatal tissue segmentation. Human Brain Mapping, 2011, 32, 382-396.	1.9	40
157	The future of acquisition speed, coverage, sensitivity, and resolution. Neurolmage, 2012, 62, 1221-1229.	2.1	40
158	An anatomically realistic temperature phantom for radiofrequency heating measurements. Magnetic Resonance in Medicine, 2015, 73, 442-450.	1.9	40
159	Highly accelerated multishot echo planar imaging through synergistic machine learning and joint reconstruction. Magnetic Resonance in Medicine, 2019, 82, 1343-1358.	1.9	40
160	Neuroimaging brainstem circuitry supporting cardiovagal response to pain: a combined heart rate variability/ultrahigh-field (7 T) functional magnetic resonance imaging study. Philosophical Transactions Series A, Mathematical, Physical, and Engineering Sciences, 2016, 374, 20150189.	1.6	39
161	Validation of diffusion MRI estimates of compartment size and volume fraction in a biomimetic brain phantom using a human MRI scanner with 300â€mT/m maximum gradient strength. NeuroImage, 2018, 182, 469-478.	2.1	39
162	Rodent Cerebral Blood Volume (CBV) changes during hypercapnia observed using Magnetic Particle Imaging (MPI) detection. NeuroImage, 2018, 178, 713-720.	2.1	39

#	Article	IF	CITATIONS
163	A 31 hannel MR brain array coil compatible with positron emission tomography. Magnetic Resonance in Medicine, 2015, 73, 2363-2375.	1.9	38
164	Impacting the effect of fMRI noise through hardware and acquisition choices – Implications for controlling false positive rates. NeuroImage, 2017, 154, 15-22.	2.1	38
165	Corpus callosum axon diameter relates to cognitive impairment in multiple sclerosis. Annals of Clinical and Translational Neurology, 2019, 6, 882-892.	1.7	38
166	Characterization of Axonal Disease in Patients with Multiple Sclerosis Using High-Gradient-Diffusion MR Imaging. Radiology, 2016, 280, 244-251.	3.6	37
167	Tilted AIPI for highly accelerated distortionâ€free EPI with point spread function (PSF) encoding. Magnetic Resonance in Medicine, 2019, 81, 377-392.	1.9	37
168	In vivo human whole-brain Connectom diffusion MRI dataset at 760 µm isotropic resolution. Scientific Data, 2021, 8, 122.	2.4	37
169	In vivo 1D and 2D correlation MR spectroscopy of the soleus muscle at 7T. Journal of Magnetic Resonance, 2010, 204, 91-98.	1.2	36
170	Sodium imaging of human brain at 7 T with 15â€channel array coil. Magnetic Resonance in Medicine, 2012, 68, 1807-1814.	1.9	36
171	The Intrinsic Shape of Human and Macaque Primary Visual Cortex. Cerebral Cortex, 2008, 18, 2586-2595.	1.6	35
172	Slice accelerated gradientâ€echo spinâ€echo dynamic susceptibility contrast imaging with blipped CAIPI for increased slice coverage. Magnetic Resonance in Medicine, 2014, 72, 770-778.	1.9	35
173	Simultaneous multislice magnetic resonance fingerprinting (SMSâ€MRF) with directâ€spiral sliceâ€GRAPPA (ds‣G) reconstruction. Magnetic Resonance in Medicine, 2017, 77, 1966-1974.	1.9	35
174	Lung Motion and Volume Measurement by Dynamic 3D MRI Using a 128-Channel Receiver Coil. Academic Radiology, 2009, 16, 22-27.	1.3	34
175	<i>T</i> ₂ -weighted 3D fMRI using <i>S</i> ₂ -SSFP at 7 tesla. Magnetic Resonance in Medicine, 2010, 63, 1015-1020.	1.9	34
176	Fast Electromagnetic Analysis of MRI Transmit RF Coils Based on Accelerated Integral Equation Methods. IEEE Transactions on Biomedical Engineering, 2016, 63, 2250-2261.	2.5	34
177	Diffusion MRI microstructure models with in vivo human brain Connectome data: results from a multiâ€group comparison. NMR in Biomedicine, 2017, 30, e3734.	1.6	33
178	A localized double-quantum filter for thein vivo detection of brain glucose. Magnetic Resonance in Medicine, 1998, 39, 651-656.	1.9	32
179	Efficacy and Safety of Pedunculopontine Nuclei (PPN) Deep Brain Stimulation in the Treatment of Gait Disorders: A Meta-Analysis of Clinical Studies. Canadian Journal of Neurological Sciences, 2016, 43, 120-126.	0.3	32
180	Multimodal Characterization of the Late Effects of Traumatic Brain Injury: A Methodological Overview of the Late Effects of Traumatic Brain Injury Project. Journal of Neurotrauma, 2018, 35, 1604-1619.	1.7	32

#	Article	IF	CITATIONS
181	7â€T MRI of the spinal cord can detect lateral corticospinal tract abnormality in amyotrophic lateral sclerosis. Muscle and Nerve, 2013, 47, 760-762.	1.0	31
182	In vivo Probabilistic Structural Atlas of the Inferior and Superior Colliculi, Medial and Lateral Geniculate Nuclei and Superior Olivary Complex in Humans Based on 7 Tesla MRI. Frontiers in Neuroscience, 2019, 13, 764.	1.4	31
183	Highâ€fidelity, highâ€isotropicâ€resolution diffusion imaging through gSlider acquisition with and T 1 corrections and integrated Δ B 0 / Rx shim array. Magnetic Resonance in Medicine, 2020, 83, 56-67.	1.9	31
184	Distortionâ€free, highâ€isotropicâ€resolution diffusion MRI with gSlider BUDAâ€EPI and multicoil dynamic B ₀ shimming. Magnetic Resonance in Medicine, 2021, 86, 791-803.	1.9	31
185	Nuclear magnetic resonance with DC SQUID preamplifiers. IEEE Transactions on Magnetics, 1989, 25, 1193-1199.	1.2	30
186	Imaging G-Ratio in Multiple Sclerosis Using High-Gradient Diffusion MRI and Macromolecular Tissue Volume. American Journal of Neuroradiology, 2019, 40, 1871-1877.	1.2	30
187	Phase maps reveal cortical architecture. Proceedings of the National Academy of Sciences of the United States of America, 2007, 104, 11513-11514.	3.3	29
188	Quality assessment of high angular resolution diffusion imaging data using bootstrap on Qâ€ball reconstruction. Journal of Magnetic Resonance Imaging, 2011, 33, 1194-1208.	1.9	29
189	Representational similarity precedes category selectivity in the developing ventral visual pathway. NeuroImage, 2019, 197, 565-574.	2.1	29
190	Dependence of resting-state fMRI fluctuation amplitudes on cerebral cortical orientation relative to the direction of BO and anatomical axes. NeuroImage, 2019, 196, 337-350.	2.1	29
191	Design analysis of an MPI human functional brain scanner. International Journal on Magnetic Particle Imaging, 2017, 3, .	1.0	29
192	Heating in the MRI environment due to superparamagnetic fluid suspensions in a rotating magnetic field. Journal of Magnetism and Magnetic Materials, 2010, 322, 727-733.	1.0	28
193	Motionâ€robust subâ€millimeter isotropic diffusion imaging through motion corrected generalized slice dithered enhanced resolution (MCâ€gSlider) acquisition. Magnetic Resonance in Medicine, 2018, 80, 1891-1906.	1.9	28
194	Comparison between 8―and 32â€channel phasedâ€array receive coils for in vivo hyperpolarized ¹³ C imaging of the human brain. Magnetic Resonance in Medicine, 2019, 82, 833-841.	1.9	28
195	Simultaneous zâ€shim method for reducing susceptibility artifacts with multiple transmitters. Magnetic Resonance in Medicine, 2009, 61, 255-259.	1.9	27
196	Realistic modeling of deep brain stimulation implants for electromagnetic MRI safety studies. Physics in Medicine and Biology, 2018, 63, 095015.	1.6	27
197	Placental MRI: Effect of maternal position and uterine contractions on placental BOLD MRI measurements. Placenta, 2020, 95, 69-77.	0.7	27
198	Safety and image quality at 7T MRI for deep brain stimulation systems: Ex vivo study with lead-only and full-systems. PLoS ONE, 2021, 16, e0257077.	1.1	27

#	Article	IF	CITATIONS
199	SAR reduction in 7T Câ€spine imaging using a "dark modes―transmit array strategy. Magnetic Resonance in Medicine, 2015, 73, 1533-1539.	1.9	26
200	A 16-channel AC/DC array coil for anesthetized monkey whole-brain imaging at 7T. NeuroImage, 2020, 207, 116396.	2.1	26
201	Use of pattern recognition for unaliasing simultaneously acquired slices in simultaneous multislice MR fingerprinting. Magnetic Resonance in Medicine, 2017, 78, 1870-1876.	1.9	25
202	Oxytocin attenuates trust as a subset of more general reinforcement learning, with altered reward circuit functional connectivity in males. NeuroImage, 2018, 174, 35-43.	2.1	25
203	Parallel transmission to reduce absorbed power around deep brain stimulation devices in MRI: Impact of number and arrangement of transmit channels. Magnetic Resonance in Medicine, 2020, 83, 299-311.	1.9	25
204	Transmit Array Spatial Encoding (TRASE) using broadband WURST pulses for RF spatial encoding in in inhomogeneous B0 fields. Journal of Magnetic Resonance, 2016, 268, 36-48.	1.2	24
205	HIgh b-value and high Resolution Integrated Diffusion (HIBRID) imaging. NeuroImage, 2017, 150, 162-176.	2.1	24
206	Design and implementation of a low-cost, tabletop MRI scanner for education and research prototyping. Journal of Magnetic Resonance, 2020, 310, 106625.	1.2	24
207	Disruption of Brainstem Structural Connectivity in <scp>REM</scp> Sleep Behavior Disorder Using 7 Tesla <scp>Magnetic Resonance Imaging</scp> . Movement Disorders, 2022, 37, 847-853.	2.2	24
208	Functional Involvement of Human Periaqueductal Gray and Other Midbrain Nuclei in Cognitive Control. Journal of Neuroscience, 2019, 39, 6180-6189.	1.7	23
209	Placental MRI. Topics in Magnetic Resonance Imaging, 2019, 28, 285-297.	0.7	23
210	Optimization of MRI Gradient Coils With Explicit Peripheral Nerve Stimulation Constraints. IEEE Transactions on Medical Imaging, 2021, 40, 129-142.	5.4	23
211	External Dynamic InTerference Estimation and Removal (EDITER) for low field MRI. Magnetic Resonance in Medicine, 2022, 87, 614-628.	1.9	23
212	Alignment of Volume MR Images and High Resolution [18F]Fluorodeoxyglucose PET Images for the Evaluation of Patients with Brain Tumors. Journal of Computer Assisted Tomography, 1997, 21, 183-191.	0.5	23
213	Bright and black blood imaging of the carotid bifurcation at 3.0T. European Journal of Radiology, 2006, 57, 403-411.	1.2	22
214	32â€channel phasedâ€array receive with asymmetric birdcage transmit coil for hyperpolarized xenonâ€129 lung imaging. Magnetic Resonance in Medicine, 2013, 70, 576-583.	1.9	22
215	Signal Fluctuation Sensitivity: An Improved Metric for Optimizing Detection of Resting-State fMRI Networks. Frontiers in Neuroscience, 2016, 10, 180.	1.4	22
216	Computation of ultimate SAR amplification factors for radiofrequency hyperthermia in non-uniform body models: impact of frequency and tumour location. International Journal of Hyperthermia, 2018, 34, 87-100.	1.1	22

#	Article	IF	CITATIONS
217	3D Echo Planar Time-resolved Imaging (3D-EPTI) for ultrafast multi-parametric quantitative MRI. NeuroImage, 2022, 250, 118963.	2.1	22
218	Brain, skull, and cerebrospinal fluid volumes in adult posttraumatic stress disorder. Journal of Traumatic Stress, 2007, 20, 763-774.	1.0	21
219	Proposing magnetic nanoparticle hyperthermia in lowâ€field MRI. Concepts in Magnetic Resonance Part A: Bridging Education and Research, 2010, 36A, 36-47.	0.2	21
220	Fourâ€dimensional spectralâ€spatial RF pulses for simultaneous correction of <i>B</i> ₁ + inhomogeneity and susceptibility artifacts in <i>T</i> ₂ *â€weighted MRI. Magnetic Resonance in Medicine, 2010, 64, 1-8.	1.9	21
221	Entorhinal verrucae geometry is coincident and correlates with Alzheimer's lesions: a combined neuropathology and high-resolution ex vivo MRI analysis. Acta Neuropathologica, 2012, 123, 85-96.	3.9	21
222	Coilâ€ŧoâ€coil physiological noise correlations and their impact on functional MRI timeâ€series signalâ€ŧoâ€noise ratio. Magnetic Resonance in Medicine, 2016, 76, 1708-1719.	1.9	21
223	Multiâ€atlas and label fusion approach for patientâ€specific MRI based skull estimation. Magnetic Resonance in Medicine, 2016, 75, 1797-1807.	1.9	21
224	Optimal experiment design for magnetic resonance fingerprinting. , 2016, 2016, 453-456.		21
225	Simultaneous Time Interleaved MultiSlice (STIMS) for Rapid Susceptibility Weighted acquisition. NeuroImage, 2017, 155, 577-586.	2.1	21
226	Concept for using magnetic particle imaging for intraoperative margin analysis in breast-conserving surgery. Scientific Reports, 2021, 11, 13456.	1.6	21
227	T1Effects in Sequential Dynamic Susceptibility Contrast Experiments. Journal of Magnetic Resonance, 1998, 130, 292-295.	1.2	20
228	Robust time-shifted spoke pulse design in the presence of large B0 variations with simultaneous reduction of through-plane dephasing, B1+ effects, and the specific absorption rate using parallel transmission. Magnetic Resonance in Medicine, 2016, 76, 540-554.	1.9	20
229	Pushing the spatio-temporal limits of MRI and fMRI. NeuroImage, 2018, 164, 1-3.	2.1	20
230	Echo-Time and Field Strength Dependence of BOLD Reactivity in Veins and Parenchyma Using Flow-Normalized Hypercapnic Manipulation. PLoS ONE, 2011, 6, e24519.	1.1	19
231	A 22â€channel receive array with Helmholtz transmit coil for anesthetized macaque MRI at 3 T. NMR in Biomedicine, 2013, 26, 1431-1440.	1.6	19
232	Ultimate MRI. Journal of Magnetic Resonance, 2019, 306, 139-144.	1.2	19
233	Phase-matched virtual coil reconstruction for highly accelerated diffusion echo-planar imaging. Neurolmage, 2019, 194, 291-302.	2.1	19
234	Model-Based Segmentation of Hippocampal Subfields in Ultra-High Resolution In Vivo MRI. Lecture Notes in Computer Science, 2008, 11, 235-243.	1.0	19

#	Article	IF	CITATIONS
235	Systematic spatial distortion in MRI due to gradient non-linearities. NeuroImage, 2001, 13, 50.	2.1	18
236	Degenerate mode birdcage volume coil for sensitivity-encoded imaging. Magnetic Resonance in Medicine, 2003, 50, 1107-1111.	1.9	18
237	Physiological noise in MR images: An indicator of the tissue response to ischemia?. Journal of Magnetic Resonance Imaging, 2008, 27, 866-871.	1.9	18
238	7T MRI of spinal cord injury. Neurology, 2012, 79, 2217-2217.	1.5	18
239	Denoising sparse images from CRAPPA using the nullspace method. Magnetic Resonance in Medicine, 2012, 68, 1176-1189.	1.9	18
240	A study-specific fMRI normalization approach that operates directly on high resolution functional EPI data at 7Tesla. NeuroImage, 2014, 100, 710-714.	2.1	18
241	Magnetic Resonance Imaging technology — bridging the gap between noninvasive human imaging and optical microscopy. Current Opinion in Neurobiology, 2018, 50, 250-260.	2.0	18
242	Individualized SAR calculations using computer visionâ€based MR segmentation and a fast electromagnetic solver. Magnetic Resonance in Medicine, 2021, 85, 429-443.	1.9	18
243	Mapping the human connectome using diffusion MRI at 300 mT/m gradient strength: Methodological advances and scientific impact. NeuroImage, 2022, 254, 118958.	2.1	18
244	Uncovering of intracellular water in cultured cells. Magnetic Resonance in Medicine, 2005, 54, 79-86.	1.9	17
245	The pulsatility volume index: an indicator of cerebrovascular compliance based on fast magnetic resonance imaging of cardiac and respiratory pulsatility. Philosophical Transactions Series A, Mathematical, Physical, and Engineering Sciences, 2016, 374, 20150184.	1.6	17
246	Fluorine spin frozen core in Pr^3+:LaF_3 observed by cross relaxation. Journal of the Optical Society of America B: Optical Physics, 1992, 9, 789.	0.9	16
247	High resolution T2-weighted imaging of the human brain using surface coils and an analytical reception profile correction. Journal of Magnetic Resonance Imaging, 1997, 7, 512-517.	1.9	16
248	Design and evaluation of a 32â€channel phasedâ€array coil for lung imaging with hyperpolarized 3â€helium. Magnetic Resonance in Medicine, 2010, 63, 456-464.	1.9	16
249	Fast Dictionary-Based Reconstruction for Diffusion Spectrum Imaging. IEEE Transactions on Medical Imaging, 2013, 32, 2022-2033.	5.4	16
250	Fast threeâ€dimensional inner volume excitations using parallel transmission and optimized kâ€space trajectories. Magnetic Resonance in Medicine, 2016, 76, 1170-1182.	1.9	16
251	Location of Subcortical Microbleeds and Recovery of Consciousness After Severe Traumatic Brain Injury. Neurology, 2021, 97, e113-e123.	1.5	16
252	Comprehensive diffusion MRI dataset for in vivo human brain microstructure mapping using 300 mT/m gradients. Scientific Data, 2022, 9, 7.	2.4	16

#	Article	IF	CITATIONS
253	Brain proton magnetic resonance spectroscopy in Alzheimer disease: changes after treatment with xanomeline. American Journal of Geriatric Psychiatry, 2002, 10, 81-8.	0.6	16
254	Measuring SPIO and Gd contrast agent magnetization using 3 T MRI. NMR in Biomedicine, 2009, 22, 891-897.	1.6	15
255	Neural Correlates of the Formation and Retention of Cocaine-Induced Stimulus–Reward Associations. Biological Psychiatry, 2012, 72, 422-428.	0.7	15
256	A 20 hannel receiveâ€only mouse array coil for a 3 T clinical MRI system. Magnetic Resonance in Medicine, 2011, 66, 582-593.	1.9	14
257	Fast reconstruction for multichannel compressed sensing using a hierarchically semiseparable solver. Magnetic Resonance in Medicine, 2015, 73, 1034-1040.	1.9	14
258	Improved 7 Tesla resting-state fMRI connectivity measurements by cluster-based modeling of respiratory volume and heart rate effects. NeuroImage, 2017, 153, 262-272.	2.1	14
259	Optimizing selective stimulation of peripheral nerves with arrays of coils or surface electrodes using a linear peripheral nerve stimulation metric. Journal of Neural Engineering, 2020, 17, 016029.	1.8	14
260	A 31 hannel integrated "AC/DC―B ₀ shim and radiofrequency receive array coil for improved 7T MRI. Magnetic Resonance in Medicine, 2022, 87, 1074-1092.	1.9	14
261	Investigating cardiac stimulation limits of MRI gradient coils using electromagnetic and electrophysiological simulations in human and canine body models. Magnetic Resonance in Medicine, 2021, 85, 1047-1061.	1.9	13
262	A 48-channel receive array coil for mesoscopic diffusion-weighted MRI of exÂvivo human brain on the 3 T connectome scanner. Neurolmage, 2021, 238, 118256.	2.1	13
263	A patientâ€friendly 16â€channel transmit/64â€channel receive coil array for combined head–neck MRI at 7 Tesla. Magnetic Resonance in Medicine, 2022, 88, 1419-1433.	1.9	13
264	Individual variation in simulated fetal SAR assessed in multiple body models. Magnetic Resonance in Medicine, 2020, 83, 1418-1428.	1.9	12
265	An integrated RF-receive/BO-shim array coil boosts performance of whole-brain MR spectroscopic imaging at 7ÂT. Scientific Reports, 2020, 10, 15029.	1.6	12
266	An efficient approach to optimal experimental design forÂmagnetic resonance fingerprinting with Bâ€splines. Magnetic Resonance in Medicine, 2022, 88, 239-253.	1.9	12
267	The â€~virtual DBS population': five realistic computational models of deep brain stimulation patients for electromagnetic MR safety studies. Physics in Medicine and Biology, 2019, 64, 035021.	1.6	11
268	An orthogonal shim coil for 3T brain imaging. Magnetic Resonance in Medicine, 2020, 83, 1499-1511.	1.9	11
269	Evaluation of RF interactions between a 3T birdcage transmit coil and transcranial magnetic stimulation coils using a realistically shaped head phantom. Magnetic Resonance in Medicine, 2020, 84, 1061-1075.	1.9	11
270	A sizeâ€adaptive 32â€channel array coil for awake infant neuroimaging at 3ÂTesla MRI. Magnetic Resonance in Medicine, 2021, 86, 1773-1785.	1.9	11

#	Article	IF	CITATIONS
271	Accelerated Diffusion Spectrum Imaging with Compressed Sensing Using Adaptive Dictionaries. Lecture Notes in Computer Science, 2012, 15, 1-9.	1.0	11
272	Dense, shapeâ€optimized posterior 32â€channel coil for submillimeter functional imaging of visual cortex at 3T. Magnetic Resonance in Medicine, 2016, 76, 321-328.	1.9	10
273	Reduction of across-run variability of temporal SNR in accelerated EPI time-series data through FLEET-based robust autocalibration. NeuroImage, 2017, 152, 348-359.	2.1	10
274	Low-field portable brain MRI in CNS demyelinating disease. Multiple Sclerosis and Related Disorders, 2021, 51, 102903.	0.9	10
275	A phased array echoplanar imaging system for fMRI. Magnetic Resonance Imaging, 1999, 17, 121-129.	1.0	9
276	Simulating magnetic nanoparticle behavior in low-field MRI under transverse rotating fields and imposed fluid flow. Journal of Magnetism and Magnetic Materials, 2010, 322, 2607-2617.	1.0	9
277	Parallel transmission pulse design with explicit control for the specific absorption rate in the presence of radiofrequency errors. Magnetic Resonance in Medicine, 2016, 75, 2493-2504.	1.9	9
278	Sensitivity analysis of neurodynamic and electromagnetic simulation parameters for robust prediction of peripheral nerve stimulation. Physics in Medicine and Biology, 2019, 64, 015005.	1.6	9
279	Scout accelerated motion estimation and reduction (SAMER). Magnetic Resonance in Medicine, 2022, 87, 163-178.	1.9	9
280	Simultaneous pure T2 and varying T2′-weighted BOLD fMRI using Echo Planar Time-resolved Imaging for mapping cortical-depth dependent responses. NeuroImage, 2021, 245, 118641.	2.1	9
281	<scp>SNR</scp> â€efficient distortionâ€free diffusion relaxometry imaging using accelerated echoâ€train shifted echoâ€planar timeâ€resolving imaging (<scp>ACEâ€EPTI</scp>). Magnetic Resonance in Medicine, 2022, 88, 164-179.	1.9	9
282	3.0 T Plaque Imaging. Topics in Magnetic Resonance Imaging, 2007, 18, 389-400.	0.7	8
283	General design approach and practical realization of decoupling matrices for parallel transmission coils. Magnetic Resonance in Medicine, 2016, 76, 329-339.	1.9	8
284	Comparison of three algorithms for solving linearized systems of parallel excitation RF waveform design equations: Experiments on an eight•hannel system at 3 Tesla. Concepts in Magnetic Resonance Part B, 2007, 31B, 176-190.	0.3	7
285	Accelerated radiation damping for increased spin equilibrium (ARISE): A new method for controlling the recovery of longitudinal magnetization. Magnetic Resonance in Medicine, 2008, 60, 1112-1121.	1.9	7
286	Array Coils. , 2014, , 59-67.		7
287	Selective magnetic resonance imaging of magnetic nanoparticles by acoustically induced rotary saturation. Magnetic Resonance in Medicine, 2016, 75, 97-106.	1.9	7
288	Rapid headâ€pose detection for automated slice prescription of fetalâ€brain <scp>MRI</scp> . International Journal of Imaging Systems and Technology, 2021, 31, 1136-1154.	2.7	7

#	Article	IF	CITATIONS
289	Optimized 64â€channel array configurations for accelerated simultaneous multislice acquisitions in 3T cardiac MRI. Magnetic Resonance in Medicine, 2021, 86, 2276-2289.	1.9	7
290	Variation of the Pr^3+ nuclear quadrupole resonance spectrum across the inhomogeneous optical line in Pr^3+:LaF_3. Journal of the Optical Society of America B: Optical Physics, 1992, 9, 784.	0.9	6
291	Simultaneous multislice magnetic resonance fingerprinting with low-rank and subspace modeling. , 2017, 2017, 3264-3268.		6
292	Chapter 52 Aids to telemetry in the presurgical evaluation of epilepsy patients: MRI, MEG and other non-invasive imaging techniques. Supplements To Clinical Neurophysiology, 2004, 57, 494-502.	2.1	5
293	Combined compressed sensing and parallel mri compared for uniform and random cartesian undersampling of K-space. , 2011, , .		5
294	Accelerated diffusion spectrum imaging with compressed sensing using adaptive dictionaries. Magnetic Resonance in Medicine, 2012, 68, spcone-spcone.	1.9	4
295	Simulations of a birdcage coil B <inf>1</inf> + field on a human body model for designing a 3T multichannel TMS/MRI head coil array. , 2018, 2018, 4752-4755.		4
296	A Huygens' surface approach to rapid characterization of peripheral nerve stimulation. Magnetic Resonance in Medicine, 2022, 87, 377-393.	1.9	4
297	Quantitative T1 and T2 mapping by magnetic resonance fingerprinting (MRF) of the placenta before and after maternal hyperoxia. Placenta, 2021, 114, 124-132.	0.7	4
298	Aspects of Clinical Imaging at 7 T. Biological Magnetic Resonance, 2006, , 59-103.	0.4	4
299	High-Resolution and Microscopic Imaging at High Field. , 2006, , 343-371.		4
300	NAA-weighted imaging of the human brain using a conventional readout gradient. Magnetic Resonance in Medicine, 1999, 41, 187-192.	1.9	3
301	Sparsity in MRI RF excitation pulse design. , 2008, , .		3
302	Evaluating sparsity penalty functions for combined compressed sensing and parallel MRI. , 2011, , .		3
303	A comprehensive diffusion MRI dataset acquired on the MGH Connectome scanner in a biomimetic brain phantom. Data in Brief, 2018, 18, 334-339.	0.5	3
304	Computer-Vision Techniques for Water-Fat Separation in Ultra High-Field MRI Local Specific Absorption Rate Estimation. IEEE Transactions on Biomedical Engineering, 2019, 66, 768-774.	2.5	3
305	Further Development of Subspace Imaging to Magnetic Resonance Fingerprinting: A Low-rank Tensor Approach. , 2020, 2020, 1662-1666.		3
306	Safety and imaging performance of two hannel RF shimming for fetal MRI at 3T. Magnetic Resonance in Medicine, 2021, 86, 2810-2821.	1.9	3

#	Article	IF	CITATIONS
307	A 128-channel head coil array for cortical imaging at 7 Tesla. , 2021, , .		3
308	Field Strength Dependence of Contrast and Noise in fMRI. Biological Magnetic Resonance, 2015, , 793-818.	0.4	3
309	A detunable elliptic transmission line resonator for body imaging at 3 Tesla. Concepts in Magnetic Resonance, 2002, 15, 92-100.	1.3	2
310	Cortical enhanced tissue segmentation of neonatal brain MR images acquired by a dedicated phased array coil. , 2009, , .		2
311	Regularizing GRAPPA using simultaneous sparsity to recover de-noised images. Proceedings of SPIE, 2011, , .	0.8	2
312	Accelerated parallel magnetic resonance imaging reconstruction using joint estimation with a sparse signal model. , 2012, , .		2
313	New Coil Systems for Highly Parallel MR Acquisition Strategies. Medical Radiology, 2007, , 497-510.	0.0	2
314	Parallel-Excitation Techniques for Ultra-High-Field MRI. Medical Radiology, 2007, , 511-521.	0.0	2
315	In Vivo Absolute Metabolite Quantification Using a Multiplexed <scp>ERETICâ€RX</scp> Array Coil for Wholeâ€Brain <scp>MR</scp> Spectroscopic Imaging. Journal of Magnetic Resonance Imaging, 2022, 56, 121-133.	1.9	2
316	22. Pharmacologic studies of brain phospholipid metabolism using MRS. Biological Psychiatry, 1998, 43, S7.	0.7	1
317	Cortical enhanced tissue segmentation of neonatal brain MR images acquired by a dedicated phased array coil. , 2009, 2009, 39-45.		1
318	Atlas-based segmentation for globus pallidus internus targeting on low-resolution MRI. , 2011, 2011, 5706-9.		1
319	Wave-CAIPI enables highly accelerated 3D MRI. , 2014, , .		1
320	Physiological noise model comparison for resting-state fMRI at 7 T. , 2016, , .		1
321	Comparison of new element designs for combined <scp>RF</scp> â€shim arrays at 7 T. Concepts in Magnetic Resonance Part B, 2018, 48B, .	0.3	1
322	Category-sensitive visual regions in human infants. Journal of Vision, 2016, 16, 204.	0.1	1
323	Rapid high spatial resolution diffusion MRI at 7 Tesla using simultaneous multislice acquisition. , 2014, , .		0
324	Nineteen-channel receive array and four-channel transmit array coil for cervical spinal cord imaging at 7T. Magnetic Resonance in Medicine, 2014, 72, spcone-spcone.	1.9	0

#	Article	IF	CITATIONS
325	Globally conditioned causality in estimating directed brain-heart interactions through joint MRI and RR series analysis. , 2015, 2015, 3795-8.		Ο
326	The Path to Parent-Inclusive Conferences. Journal of the American College of Radiology, 2021, 18, 334-336.	0.9	0
327	Modeling of cardiac stimulation by externally applied electromagnetic fields. , 2021, , .		Ο
328	Techniques for Brain Functional Connectivity Analysis from High Resolution Imaging. Studies in Computational Intelligence, 2015, , 131-138.	0.7	0
329	Multimodal Registration of White Matter Brain Data via Optimal Mass Transport. , 2008, 2008, 27-35.		ο